Performance of the GSN station RPN-II, 1988-2009

A report in a series documenting the status of the Global Seismographic Network

WQC Report 2010:8
February 27, 2010

Göran Ekström and Meredith Nettles

Waveform Quality Center
Lamont-Doherty Earth Observatory of Columbia University, New York

1 Station performance report: RPN

This report summarizes a number of observations that are relevant for assessing the past and current quality of the data recorded at one of the stations of the Global Seismographic Network. The purpose of the report is, in part, to document specific problems observed with the data. Some of these problems are related to errors in the available descriptions of station parameters: orientation of the sensors, response functions, polarities. In principle, such errors in the station metadata can be corrected by providing updated station parameters. In practice, this may be difficult in some cases due to lack of knowledge of, or inability to determine, the correct parameters. Other problems are caused by the malfunctioning of some instrument component. Regardless of the cause, it is necessary to document and publicize the lack of accurate and reliable station characteristics, especially when it is not obvious from simple inspection of the data that a problem exists. It is also of value to document the characteristics of stations performing well, both to establish their high quality and to help identify installation and operation procedures that should be emulated at other stations.

1.1 Station RPN

The station RPN (Rapa Nui) is located on Easter Island in the South Pacific (see Figure 1). It lies close to the earthquake activity along the East Pacific Rise and the Easter Microplate to the west, and to intraplate earthquakes associated with the Easter hotspot.

RPN is one of the most isolated GSN stations; the closest GSN station is PTCN-IU (Pitcairn), more than 2000 km to the West. RPN is in an excellent location for providing global coverage in earthquake and Earth structure studies.

RPN is part of the IDA (II) component of the IRIS/USGS Global Seismographic Network and is operated by the IDA group at the University of California, San Diego.

1.2 The data

Digital seismic data from RPN are available from the IRIS DMC beginning in 1988. Here, we consider broadband instruments at the station. The initial installation in 1987 consisted of a set of STS-1 seismometers. An auxiliary STS-2 sensor was installed in 2002. Data from RPN are included in our standard CMT analysis (Dziewonski et al., 1981; Ekström et al., 2005), and waveform data, travel-time observations, and dispersion curves derived from RPN data have been used in the development of numerous global and regional tomographic models since the station was installed.

In the analyses described here, we have made use of data collected from the IRIS DMC. We requested and downloaded all long-period (LH) and very-long-period (VH) data available at the DMC for both sensors from 1988 until until September 2009. Data for 1987 are not available at the IRIS DMC. We used the currently available station metadata prepared by the IDA group in San Diego (downloaded in December 2009) and also available at the IRIS DMC. Overall, the station has been operated with few data outages since 1988.

1.3 The metadata

The dataless SEED volume for RPN documents 7 response epochs for the STS-1 (primary) and STS-2 (secondary) sensors at RPN. The STS-1 1 sps LH channels have location code 00 and we refer to these channels as LHZ-00, LHN-00, and LHE-00. The STS-2 sensor (location code 10) was installed on 2002.260 (260 representing the day of year) and we refer to the 1 sps channels as LHZ-10, LHN-10, and LHE-10. Epoch boundaries are given at 1987.166 (STS-1 installed), 1988.014, 1990.150, 1992.343, 1994.043, 2002.260 (first STS-2 data), and 2003.080. The metadata indicate gain changes at all epoch boundaries as well as small changes in the frequency response.

1.4 Scaling analysis

One method for assessing the quality of the data is the systematic comparison of recorded long-period waveforms with synthetic seismograms calculated for known seismic events. This analysis follows the steps described by Ekström et al. (2006). Seismic data for the LH and VH channels from both the STS-1 and STS-2 sensors are collected. Corresponding synthetic waveforms for all earthquakes in the Global CMT catalog (Dziewonski et al., 1981; Ekström et al., 2005) with $M_W \geq 6.5$ are calculated. Correlation coefficients and optimal scaling factors between observed and synthetic waveforms are calculated for the three types of data used in the standard CMT analysis: body waves (B), with periods in the range 50–150 sec, mantle waves (M), with periods in the range 125–350 sec, and surface waves (S), with periods in the range 50–150 sec. Body- and mantle-wave results are discussed here. The scaling factor is only calculated for waveforms with a correlation of 0.75 or greater. The scaling factor is the number by which the synthetic seismogram should be multiplied to maximize the agreement with the observed seismogram. Annual median values of the scaling factors are calculated when four or more individual event scaling estimates are available for the year. Reversed components can be identified by their large negative correlations.

Figure 2 shows the results of our systematic comparison of RPN waveforms with synthetic seismograms. From 1988 until the present, both the STS-1 and STS-2 signals for large earthquakes correlate well with synthetic waveforms. There exists an average offset in the amplitudes for body waves such that synthetic seismograms should, on average, be multiplied by a factor close to 0.8 to maximize the fit to the observed waveforms. Since results are consistent for both sensors, we interpret this as a structural effect: many paths to RPN are purely oceanic, which may provide an explanation. We also note that a similar offset is seen at KIP-IU (Ekström and Nettles, WQC Report 2010:2), which is in a similar oceanic setting.

1.5 Noise analysis

A second method for investigating the overall performance of the sensors is to monitor background noise levels for all seismic channels, after conversion of the data to ground acceleration. We calculate hourly rms values of the time-domain seismic signal in narrow frequency bands, and convert the rms values to a power spectral density (PSD) at that frequency using Parseval's theorem. For each month, we then calculate the low-noise value at each frequency by determining the PSD amplitude not exceeded 10% of the time.

The PSD data provide much information about the station and the sensors. Figure 3 shows the monthly low-noise estimate for each LH channel at 193-s period since 1988. The first observation is that the station has been providing data without major outages since 1988. STS-1 noise levels have largely been stable, with a few exceptions: the vertical component was quite noisy before 1990, and had a three-year-long period of greater noise levels around 1998. Horizontal noise levels are relatively high, presumably because of the island location, but have been stable throughout the period of operation. Some monthly measurements for the N–S component after 2008 are unusual with both very low and very high values. Maintenance notes on the IDA web site (http://ida.ucsd.edu/Stations) discuss a problem with the N–S sensor starting in late 2008.

The noise level on the STS-2 seismometers shows somewhat erratic behavior, especially on the vertical component. This STS-2 sensor has recently (February, 2010) been replaced according to the IDA web site (http://ida.ucsd.edu/Stations).

1.6 Inter-sensor coherence

An additional method for assessing the quality and calibration of the recorded signals is to calculate inter-sensor coherence. This analysis is possible when more than one sensor is operated in the same location. At RPN, this is possible for the period 2002–2009, during which time both STS-1 and STS-2 instruments have operated.

We calculate the coherence of the deconvolved vertical, N–S, and E–W components. The coherence is calculated for $\sim$2-hour-long time windows containing the signals for earthquakes with $M_W \geq 6.5$ (the same events used in the scaling analysis). For each pair of seismograms, the coherence is calculated in narrow frequency bands around 32 s, 64 s, 128 s and 256 s. If the coherence is greater than 0.95, the value is stored together with the complex scaling factor (represented here as a scaling factor and phase shift) that should be applied to the secondary-sensor data to bring the two time series into the best agreement. In the following, the discussion is based on the assumption that the secondary (STS-2) sensor is properly calibrated and that deviations from a scaling factor of 1.0 and a phase shift of 0° should be attributed to differences between the true and reported response functions of the primary (STS-1) sensor.

Figure 4 shows the results of the coherence analysis for the vertical component. The measurements are very consistent and stable, with a scaling factor close to 1.0 for all periods, and a phase shift close to 0°. Nearly all scaling values are slightly larger than 1.0, suggesting that the true gain of the STS-1 may be 1–3% greater than stated in the metadata. No measurements are available after April 2009 due to the malfunction of the STS-2 sensor.

The horizontal components show results similar to those of the vertical. Figure 5 shows the amplitude and phase differences for the N–S components. A scatter of scaling measurements corresponding to gain variations of a few percent is seen. A small offset, consistent with a lower gain for the STS-1 than reported, is also seen on this component. No temporal trend is apparent. The lack of coherence measurements at 256-s period is probably related to the high noise level at the station. No measurements are available after October 2008 due to the malfunction of the STS-1 sensor (http://ida.ucsd.edu/Stations) and, subsequently, the STS-2 sensor.

Figure 6 shows the results for the E–W component, which are similar to those of the N–S component. In general, the measurements are consistent with stable instrument responses during the time period. No measurements are available after April 2009 due to the malfunction of the STS-2 sensor. A small offset, consistent with a lower gain for the STS-1 than reported, is also seen on this component.

1.7 Polarization analysis

The orientation of the horizontal components can be assessed empirically by comparing observed and synthetic waveforms, and finding the angle by which the horizontal components should be rotated in order to maximize the agreement. We follow the approach described by Ekström and Busby (2008) for such a comparison, using the observed and synthetic waveforms from Global CMT analysis.

We apply the method of Ekström and Busby (2008) to the same dataset used in the scaling analysis. Figure 7 shows the individual measurements for the period of operation for the different channels. The median rotation angle is -2° for the STS-1 and 0° for the STS-2, and the spreads of the observations are small, for both sensors. The median estimates for the entire period of operation are given in Table 1.

Comp. 1	Comp. 2	First	Last	# Obs.	N	Az 1	Az 2	25%	Med.	75%
LHE-00	LHN-00	19880112	20090902	613	138	90	0	-5	-2	1
LHE-10	LHN-10	20021003	20090902	290	53	90	0	-3	0	3

Table 1: Statistics of sensor-rotation angles estimated in this study. Columns are the channel names, the dates of the first and last observations considered in making the estimate, the total number of observations, the number of observations of acceptable quality, the reported azimuths of sensitivity of the two channels, the median polarization-angle deviation from the reported orientation together with the range of the second (25%) and third (75%) quartiles of the observations.

1.8 Example seismograms

The anomalies described here agree with observations we have made in our routine analysis of waveforms for the determination of CMT earthquake parameters. When confronted with the seismograms for an individual earthquake, it is often difficult to assess whether a poor fit is due to incorrect source parameters, inadequate modeling of wave propagation through an Earth model, or some problem with the recorded seismograms. Here, we have included some examples of data that illustrate the characteristics of the types of problems that we have encountered with data from the RPN station.

Figure 8 shows an example of three-component mantle-wave data for an earthquake on March 20, 2008. The top panel shows seismograms recorded on the STS-1 sensor and corresponding synthetic waveforms. The fit is very good. The bottom panel shows the seismograms and synthetic waveforms for the STS-2 sensor. The fit is equally good for the STS-2 sensor.

Figure 9 shows observed and synthetic body-wave seismograms for an earthquake on January 3, 2009. The top panel shows seismograms for the STS-1 sensor. The fit is good for the vertical and E–W components, but the N–S component is not seismic. Bottom panel shows seismograms recorded on the STS-2 sensor. The fit is reasonable for all three components. Figure 10 shows observed and synthetic surface-wave seismograms for an earthquake later in 2009 (July 15). The top panel shows STS-1 seismograms, for which the fit is very good for all three components. The bottom panel shows the seismograms recorded on the STS-2 sensor, for which the signals are not seismic.

2 Summary and analysis

At the time of writing (February, 2010), the GSN station RPN is performing relatively well. During the last year, there have been problems with both sensors that have resulted in the replacement of some equipment (as reported on the IDA web site). In general, our analysis suggests that the station has produced high-quality data consistently since 1988, and that the STS-2 has provided backup data streams of reasonable quality for most of the period since 2002.

The results from coherence analysis suggest a relative gain difference of 1-3% between the STS-1 and STS-2, with too-small gain specified for the vertical STS-1, and too-large gain specified for the horizontal components. Low-amplitude variations are seen in the coherence analysis of the horizontal components, but these are small. We do not understand fully the larger scatter (still small) of coherence measurements for the horizontal components compared with those of the vertical components.

3 Conclusions and recommendations

This analysis shows that RPN generally generates data of high quality. While more detailed analysis would be required to establish that the response characteristics are accurate to within the 1% tolerance of the GSN design goals (IRIS, 1985; Lay et al., 2002), our assessment is that, at least at long periods, RPN generates GSN-quality data and has done so consistently since 1988.

We note that there is no indication that the STS-1 at RPN is suffering from the long-period gain loss documented at several other stations equipped with STS-1 seismometers (Ekström et al., 2006). To the extent that it is possible to identify installation details or operational procedures that could have contributed to the elimination (or delayed onset) of this problem, it would be useful to document these and modify other installations accordingly.

We also note that the earliest (pre-1988) broadband data from RPN are not available from the IRIS DMC.

4 References

Dziewonski, A. M., T.-A. Chou, and J. H. Woodhouse, Determination of earthquake source parameters from waveform data for studies of global and regional seismicity, *J. Geophys. Res.*, 86, 2825–2853, 1981.

Ekström, G., A. M. Dziewonski, N. N. Maternovskaya, and M. Nettles, Global seismicity of 2003: Centroid-moment tensor solutions for 1087 earthquakes, *Phys. Earth Planet. Inter.*, 148, 327–351, 2005.

Ekström, G., C. A. Dalton, and M. Nettles, Observations of time-dependent errors in long-period gain at global seismic stations, *Seism. Res. Lett.*, 77, 12–22, 2006.

Ekström, G., and R. W. Busby, Measurements of seismometer orientation at USArray Transportable and Backbone stations, *Seism. Res. Lett.*, 79, 554-561, 2008.

Ekström, G., and M. Nettles, Performance of the GSN station KIP-IU, 1988–2009, Waveform Quality Center Report 2010:2, 2010.

IRIS, *The design goals for a new global seismographic network*, IRIS GSN committee report, 31 pages, 1985.

Lay, T., J. Berger, R. Buland, R. Butler, G. Ekström, B. Hutt, B. Romanowicz, *Global seismic network design goals update 2002*, IRIS GSN committee report, 2002.

Peterson, J., Observations and modeling of background seismic noise, *U. S. Geol. Surv. Open-file Rep. 93-322*, 1–45, 1993.

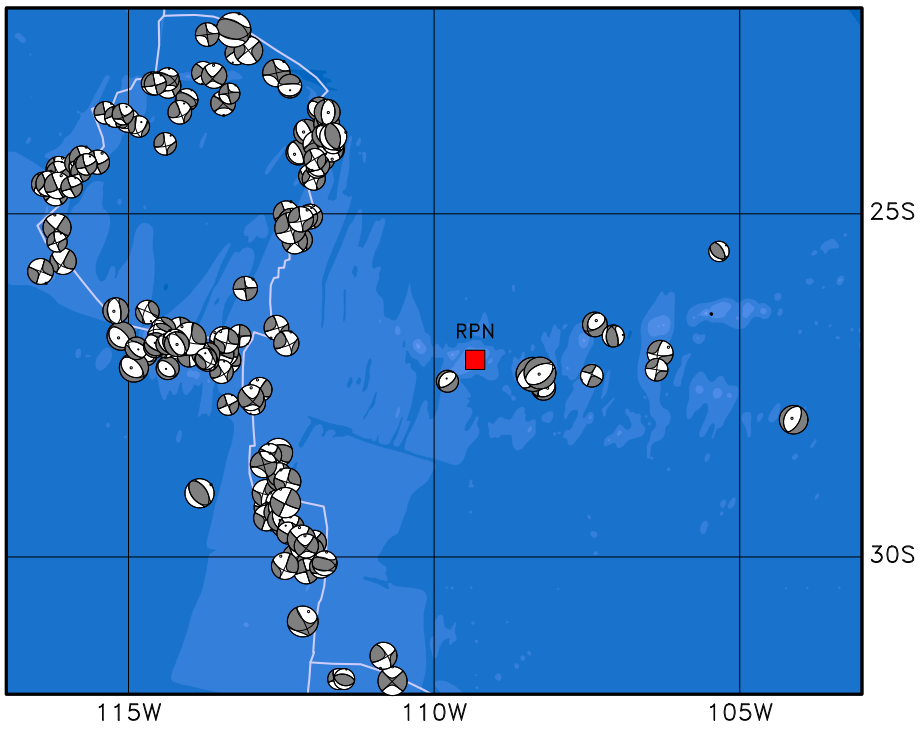

Figure 1: Map showing the location of RPN (red square) on Easter Island. Grey focal mechanisms show the locations and moment tensors of earthquakes in the Global CMT catalog. The closest GSN station is PTCN-IU, located ∼2000 km to the west on the island of Pitcairn.

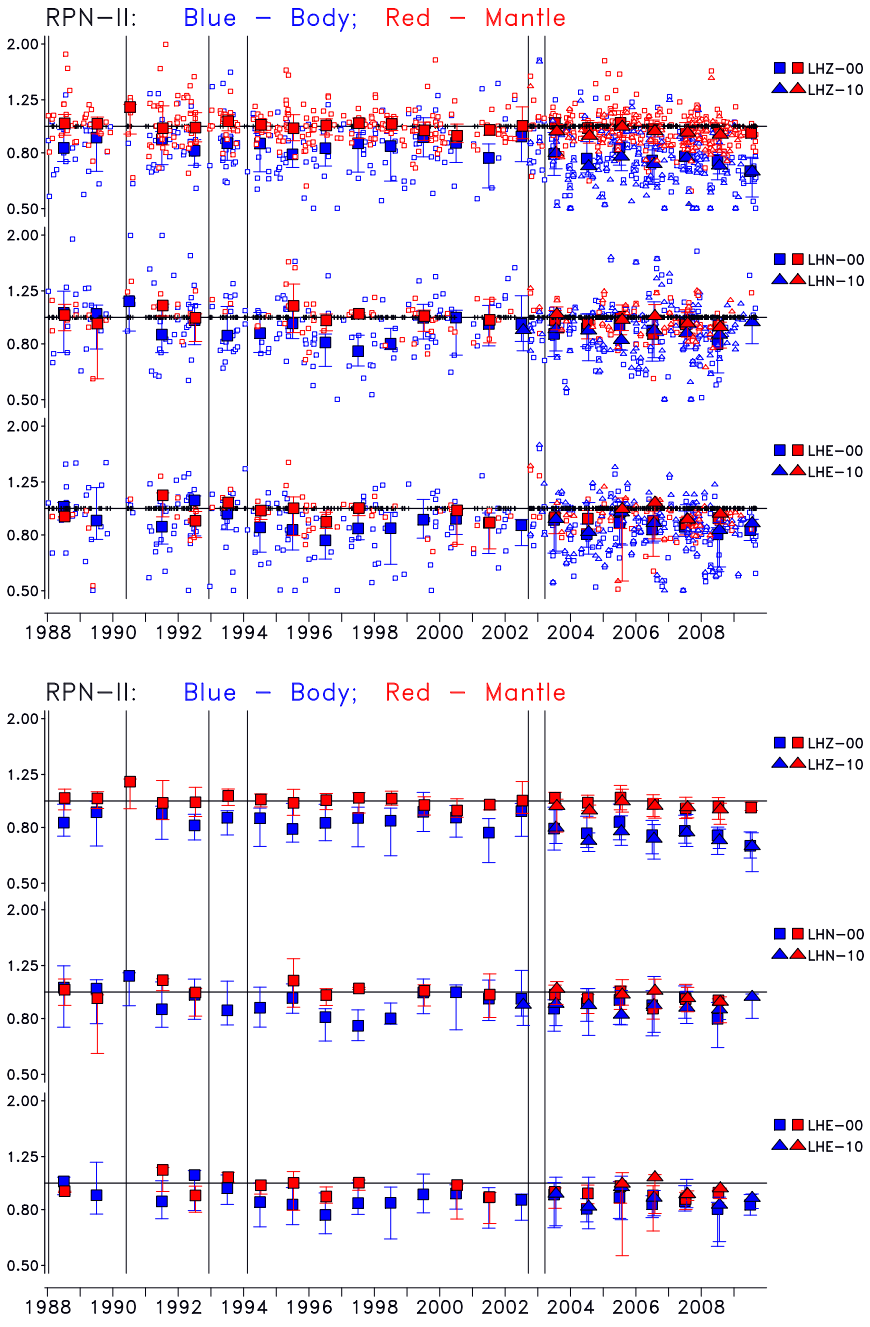

Figure 2: Scaling factors for the various data channels at RPN. Small symbols in top panel show scaling factors for individual traces. Tick marks on the horizontal axes show times of observations for which the correlation was less than 0.75. Large symbols show the median scaling factor for each year, with the error bars corresponding to the range of the second and third quartiles of the scaling factors. The legend on the right identifies the symbol type with a specific channel. Thin vertical lines show the response epoch boundaries present in the metadata. Bottom panel: same, but showing only the annual median values. The offset of body-wave values from 1.0 for both sensors may be the result of Earth structure.

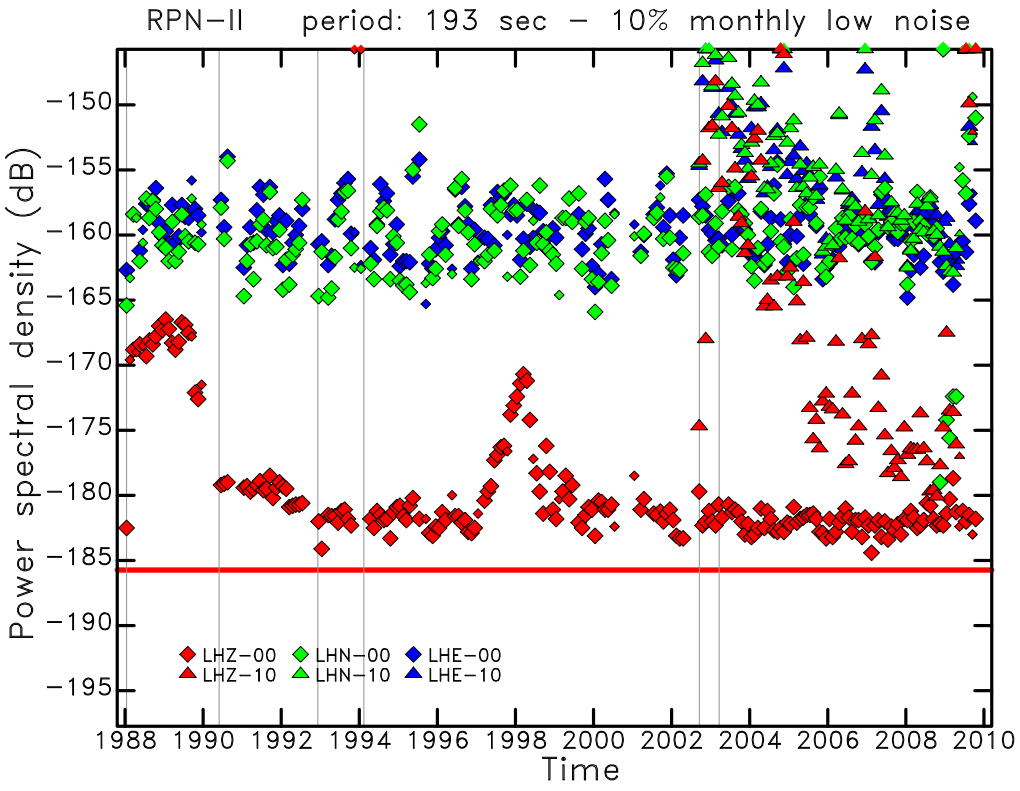

Figure 3: Monthly PSD of ground acceleration at 193-s period for all long-period (LH) channels at RPN for the period 1988–2009. Smaller symbols are used for months with fewer available hourly measurements. Each component and sensor is represented by a distinct symbol and color. The red horizontal line indicates the level of Peterson's (1993) Low Noise Model (LNM) at 193 s. The thin vertical lines show the times of epoch boundaries in the station metadata.

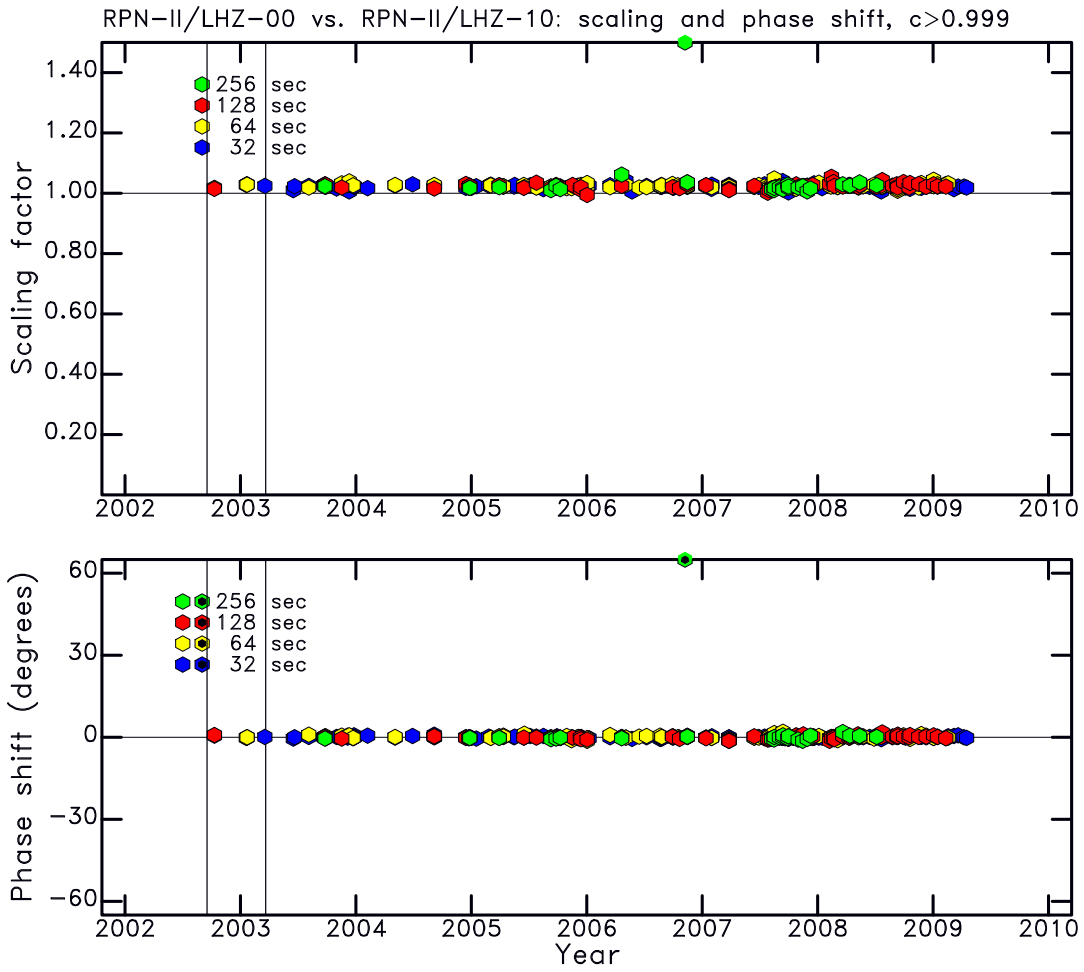

Figure 4: Diagram shows the result of coherence analysis for the vertical components of the STS-1 and STS-2 sensors. Each symbol represents a measurement of coherence for a $M_W \geq 6.5$ earthquake. The minimum coherence plotted is indicated by c. The scaling and phase shift between the two time series is shown at four different periods. The small deviations of the coherence measurements from a scaling of 1.0 and a phase shift of 0° show that the calibrations are consistent. The thin vertical lines show the times of epoch boundaries in the station metadata.

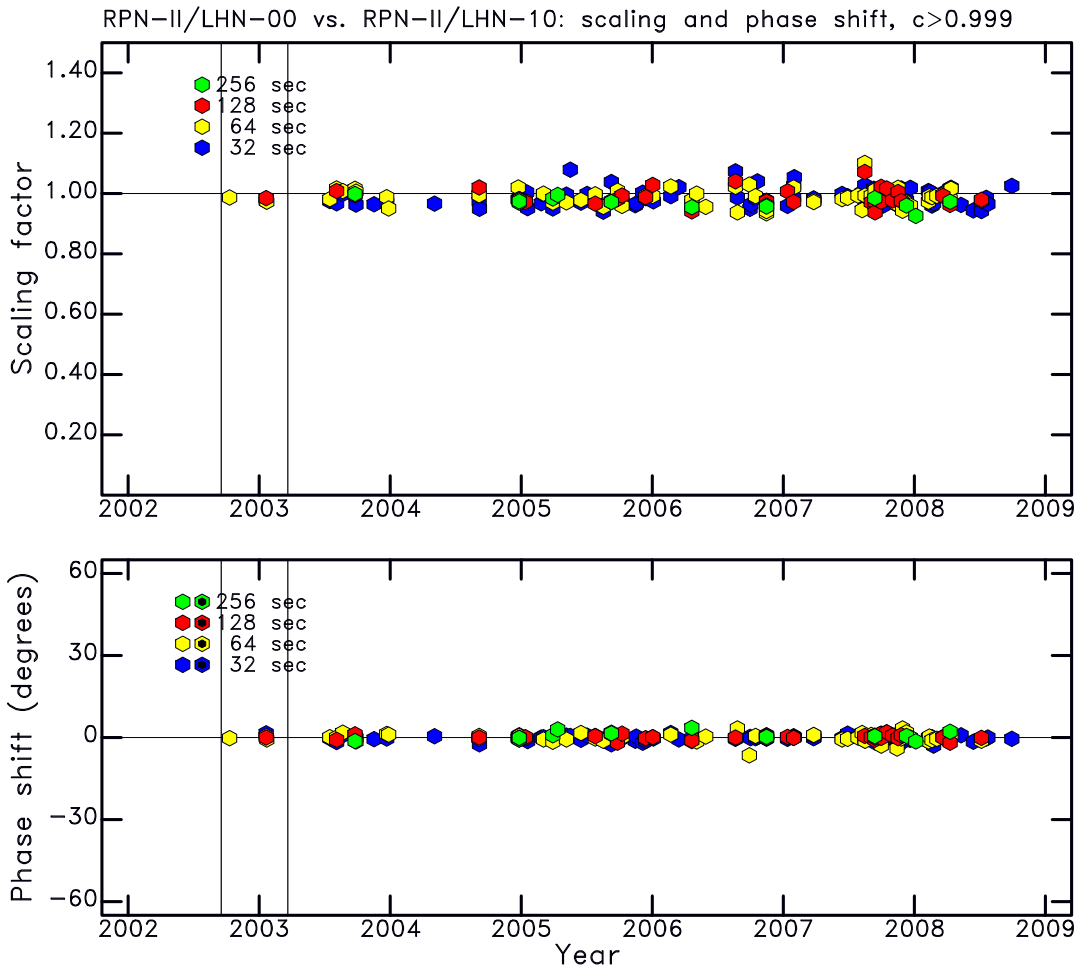

Figure 5: Same as Figure 4, but for the North-South components. No measurements are available after October 2008 due to problems with the STS-1 sensor and, after April 2009, the STS-2 sensor.

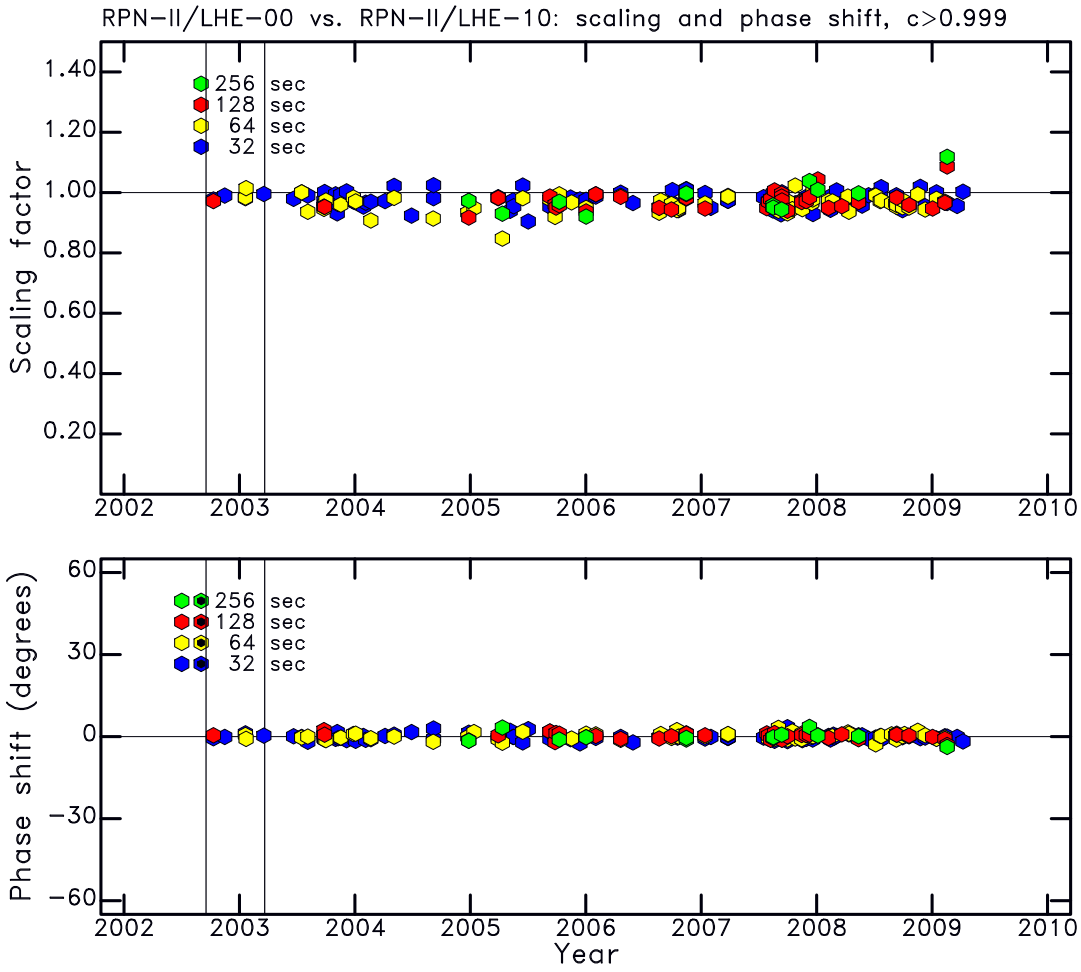

Figure 6: Same as Figure 4, but for the East-West components.

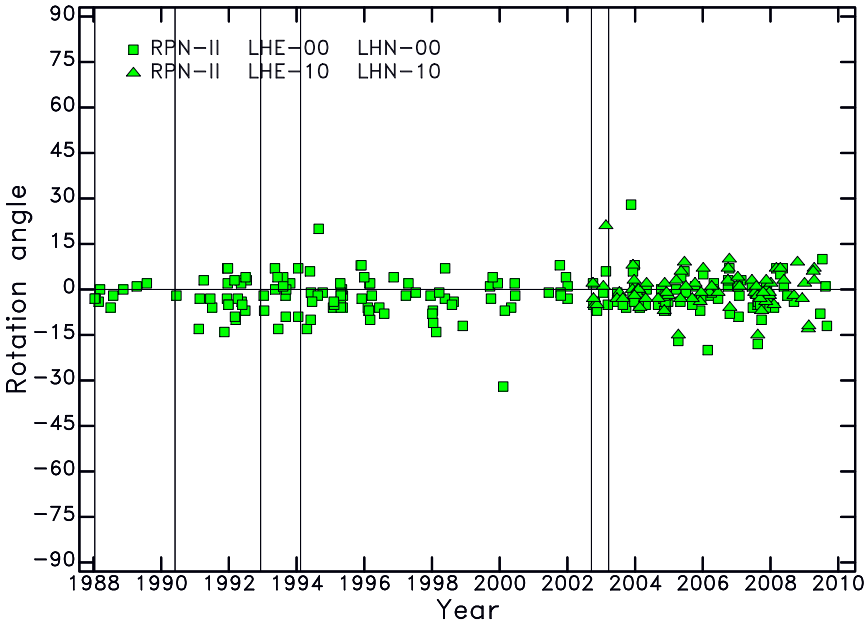

Figure 7: Individual measurements of polarization angle as a function of time. All measurements for the period of operation are shown. Symbols represent measurements obtained in the surface-wave band of the CMT analysis. More than 50% of the observations lie in the range -5° to $+1^\circ$ for the STS-1 sensor and in the range -3° to 3° for the STS-2 sensor. The thin vertical lines show the times of epoch boundaries in the station metadata.

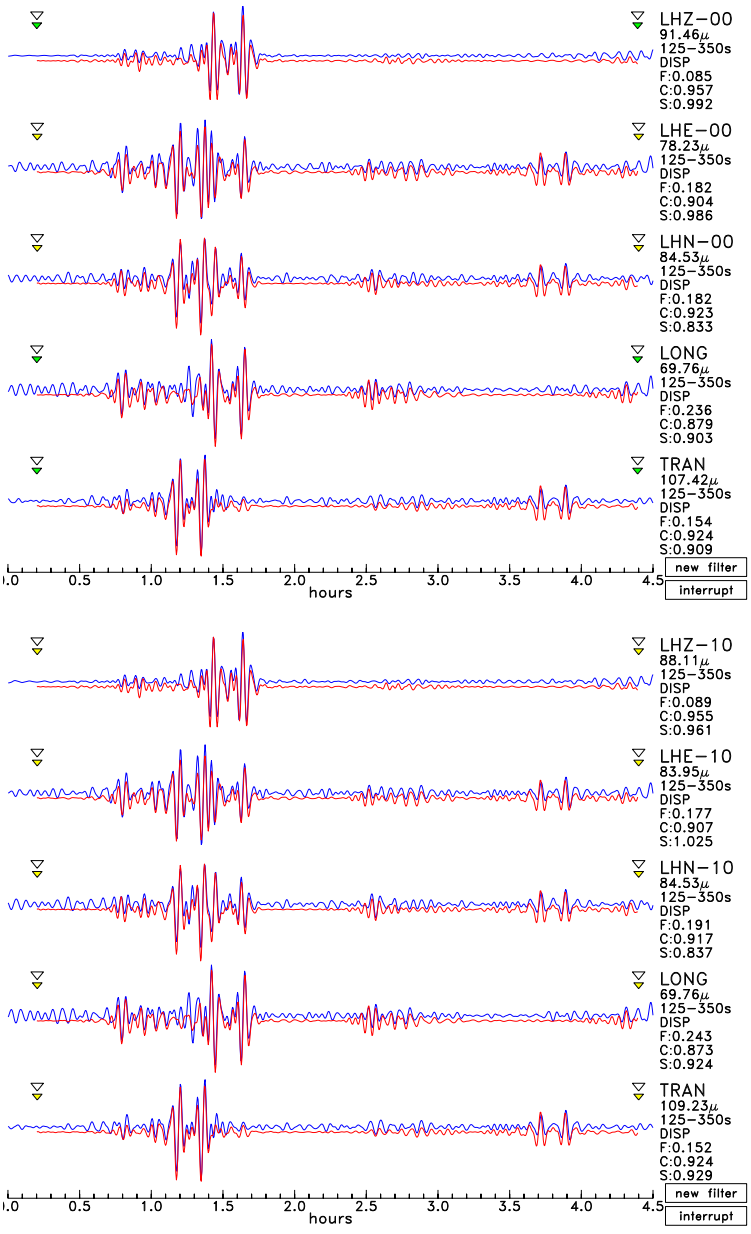

Figure 8: (Top) Observed (STS-1) and synthetic mantle-wave seismograms for an earthquake ($M = 7.1$) on March 20, 2008. The fit is very good. (Bottom) Observed (STS-2) and synthetic mantle-wave seismograms for the same earthquake, but recorded on the STS-2 seismometer. The fit to all three components is very good, and the scaling factors for each component are similar to those of the corresponding STS-1 seismograms.

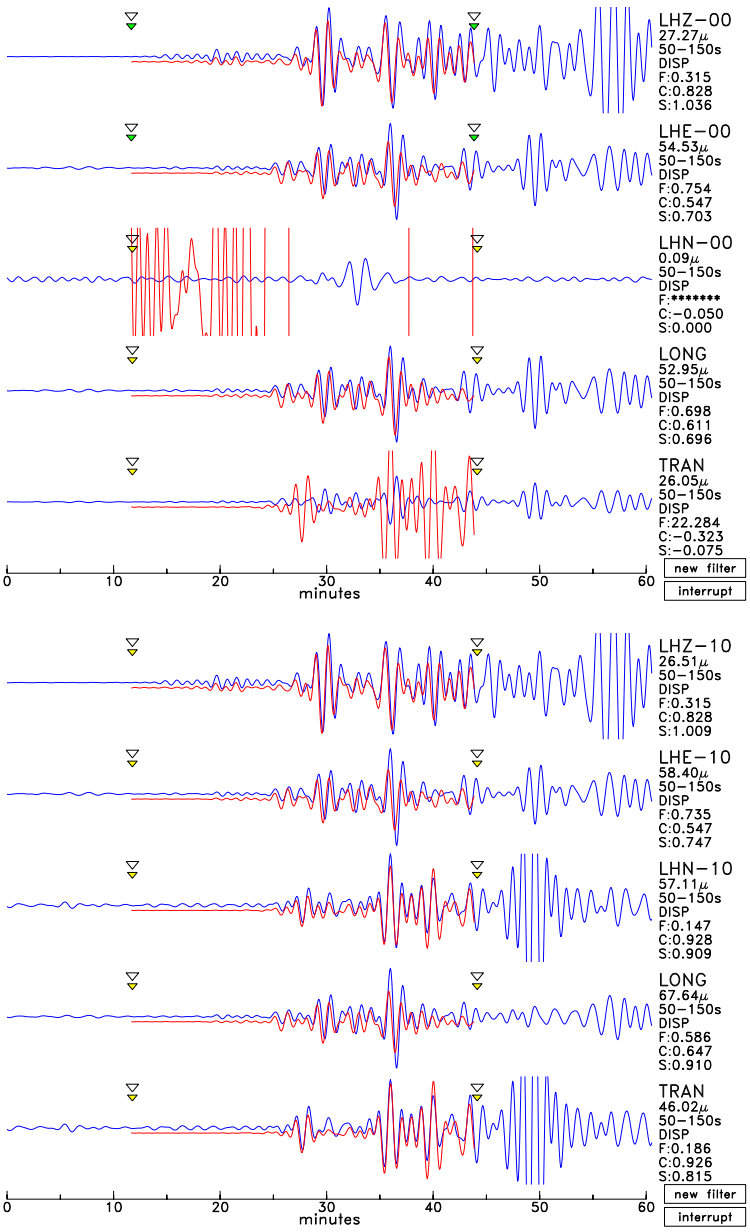

Figure 9: (Top) Observed (STS-1) and synthetic body-wave seismograms for an earthquake on January 3, 2009. The fit is good on the vertical and E–W components. The N–S signal is not seismic, as reported in the station-maintenance notes on the IDA web site. (Bottom) Observed (STS-2) and synthetic body-wave seismograms for the same earthquake, but recorded on the STS-2 seismometer. The fit to all three components is reasonable, and the scaling factors for the vertical and E–W components are very similar to those of the corresponding STS-1 seismograms.

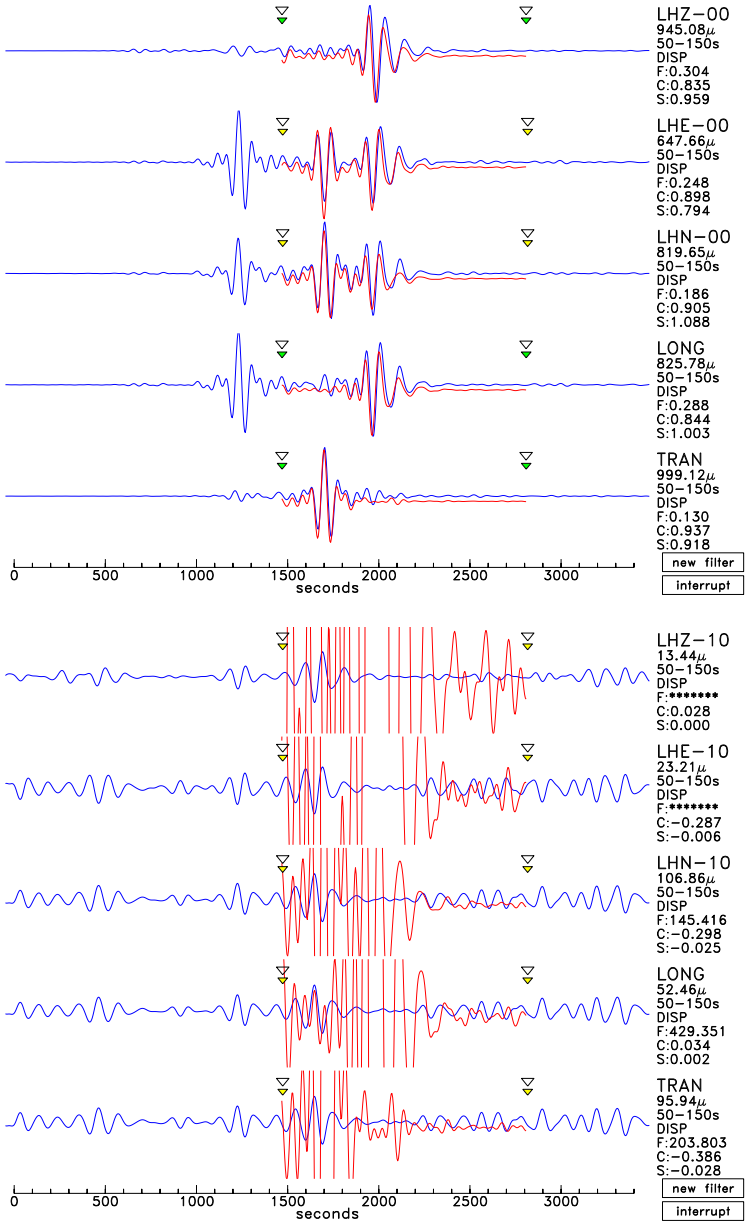

Figure 10: (Top) Observed (STS-1) and synthetic surface-wave seismograms for an earthquake on July 15, 2009. The fit is very good. (Bottom) Observed (STS-2) and synthetic surface-wave seismograms for the same earthquake, but recorded on the STS-2 seismometer. The signal is not seismic.